Metrol. Meas. Syst., Vol. 32 (2025) No. 2, pp. 1–17
DOI: 10.24425/mms.2025.154343

PAN
POLSKA AKADEMIA NAUK

METROLOGY AND MEASUREMENT SYSTEMS

Index 330930, ISSN 0860-8229
www.metrology.wat.edu.pl

M&MS

RESEARCH ON AN IMPROVED ANT COLONY ALGORITHM FOR OPTIMIZING THE INSPECTION PATH OF FREE-FORM SURFACES

Yueping Chen[1)], Sian Wei[1)], Jiegao Ma[2)]

1) Guangxi University of Science and Technology, School of Mechanical and Automotive Engineering, Liuzhou, China
2) Dongfeng Liuzhou Motor Co., Ltd, Liuzhou, China (✉ *739618159@qq.com*)

Abstract

To address the disordered inspection paths and long inspection time encountered when coordinate measuring machines (CMMs) inspect free-form surface parts, an improved ant colony algorithm was proposed to optimize the inspection path and thereby improve inspection efficiency. To enhance the optimization performance of the ant colony algorithm and overcome its shortcomings, such as low search speed and susceptibility to local optimal solutions, this work improves the initial pheromone distribution, pheromone evaporation factor, and pheromone update strategy and introduces a local search strategy. The experimental results revealed that the improved ant colony algorithm had strong search directionality in the early stages of iteration, higher search speed, and an enhanced ability to escape from local optimal solutions; the inspection paths of the free-form surface optimized by the improved ant colony algorithm were neat and aesthetically pleasing, and the inspection efficiency increased by up to 14.75%, 23.59%, and 34.21% compared with those of the classic ant colony algorithm, artificial bee colony algorithm, and genetic algorithm, respectively.

Keywords: free-form surface, path planning; ant colony algorithm, coordinate measuring machine.

1. Introduction

Free-form surfaces find extensive application across multiple sectors, including but not limited to aeronautics, tooling, automotive, and medical industries, owing to their varied configurations and other contributing aspects [1]. *Coordinate measuring machines* (CMMs) are commonly used for inspecting the size and shape accuracy of free-form surface parts to determine whether they meet the expected requirements because of their high inspection accuracy and simple operation. When CMMs are used to inspect free-form surfaces, the number of *measurement points* (MPs), the arrangement strategy of the MPs, and the quality of the *inspection path* (IP) plan are important factors that determine the inspection efficiency. Consequently, it is essential to devise an optimal IP for the MPs prior to conducting the inspection. The number and distribution of MPs determine the effectiveness of the inspection (that is, whether the inspection results can reflect the form error of free-form surfaces). The optimization of the IP does not affect the effectiveness of the inspection.

Article history: received November 10, 2024; revised February 16, 2025; accepted March 23, 2025; available online April 29, 2025.

The purpose of optimizing the IP is to further improve the inspection efficiency. Therefore, this paper does not use the inspection results (the form error of free-form surfaces) as an indicator to evaluate the performance of the proposed algorithm. Instead, the experiments are conducted under the hypothetical condition of using 100, 200, and 300 randomly distributed MPs.

In order to effectively improve the inspection efficiency of CMMs, many scholars have conducted in-depth research on the number and layout of MPs. Kamrani *et al.* [2] determined the number and position of MPs for prismatic parts and some axially symmetric parts through methods such as feature recognition and accessibility analysis. Abdulhameed *et al.* [3], basing on node vectors, divided surfaces into regions of different complexities and recursively determined the number and distribution of MPs in each region according to curvature, effectively reducing the number of MPs to improve inspection efficiency. He *et al.* [4] proposed an adaptive sampling strategy based on a machining error model, which improved both inspection efficiency and accuracy.

At the same time, a large number of scholars have improved the inspection efficiency of CMM for free-form surfaces through path optimization. For example, Virgil *et al.* [5] used an optimization algorithm based on matrix relaxation and the nearest neighbour method to optimize the IP of car bodies, which significantly improved inspection efficiency. Li and colleagues [6] introduced an enhanced search algorithm that leverages the concepts of adjacent feature mapping and convex hulls, which performed well in IP planning for structural aerospace parts and effectively avoided collisions. Liu *et al.* [7] used a local path generation method based on the probe trajectory and its rotation to quantify the *inspection time* (IT) in the IT matrix, this led to a substantial enhancement in the inspection process of free-form surface components and substantially diminished the count of virtual points required. And a hybrid path optimization algorithm based on *ant colony optimization* (ACO) and *genetic algorithm* (GA) was proposed by Tsagaris, which reduced the IT by 50% compared with the GA [8]. Yi *et al.* [9] introduced an all-inclusive strategy for optimizing the IPs of free-form surfaces, which employs a specialized algorithm to expedite the computation of the probe's reachability cone using graphical processing capabilities. This method effectively reduced the number of rotations of the probe head by grouping the MPs that use the same inspection posture and inspecting them in order, thereby shortening the IT. Li *et al.* [10] divided the MPs into different regional groups on the basis of the orientation relationship of the points to be measured and optimized the IP of the points within the group via the Lin–Kernighan algorithm, whereas the path between the groups was globally optimized via the greedy algorithm. Although the optimized IP was significantly shortened, the probability of this algorithm getting into a local optimal solution was relatively high.

Abdulhameed *et al.* [11] combined artificial neural networks with GAs and applied them to the optimization of IPs for free-form surfaces, which shortened the IP by approximately half and greatly improved the inspection efficiency. Han *et al.* [12] applied the ACO to local path optimization and optimized multitarget inspection through a path reoptimization algorithm, which significantly improved the CMM inspection efficiency and achieved an intelligent inspection process. Stojadinovic *et al.* [13] optimized the IP of prismatic workpieces via the ACO and proposed an inspection model for prismatic parts via a CMM, which effectively improved the inspection efficiency; however, the model was limited to prismatic parts and had a large limitation. Zhao and colleagues [14] utilized the ACO to refine the IP for substantial surface components, demonstrating a reduction in IP length and an increase in inspection efficiency when contrasted with the conventional zigzag algorithm. Zakharov *et al.* [15] used the ACO to optimize the trajectory length of the probe to minimize it and to effectively reduce the time cost when the CMM inspects parts and compared it with the branch and bound algorithm in experiments. The experiments revealed that the solution optimized by the ACO was closer to the optimal solution, and the optimization process took less time, indicating that the inspection efficiency of the CMM was effectively improved. He and team [16] harnessed the Kuhn–Munkres algorithm to refine the IP for enhanced CMM safety and efficiency. They introduced an automatic collision inspection algorithm which proved adept at preventing probe-to-part collisions during the inspection. Zhao *et al*. [17] proposed a high-efficiency comprehensive IP optimization method through the exploration of the random tree algorithm and GA for multinode search, which included the calculation algorithm for the inspection direction cone and probe reachability cone, classified the MPs to be measured, and finally applied the method to the five-axis coordinate-measuring machine, which effectively improved the inspection efficiency. Han *et al*. [18] used the ACO for local and global IP optimization and proposed a spherical model for collision inspection and avoidance in the inspection process. Empirical results demonstrated that the approach significantly enhanced both the efficiency and safety of the measurement process using the machine. Lin *et al*. [19] proposed a workpiece inspection system based on 3D graphic scanning recognition of MP coordinates, in which the *adaptive group-based differential evolution* (AGDE) algorithm proposed for optimization of the IP integrated the concept of grouping and determined the search method in the algorithm search iteration process by referring to the optimal solution for each group, thereby effectively improving the local search ability and overall search efficiency. The experiments revealed that the above method could obtain the shortest collision-free IP, ensuring a high-efficiency inspection process under safe inspection conditions.

The path planning problem of free-form surface MPs is actually also a combinatorial optimization problem. In the realm of combinatorial optimization challenges, the well-known *travelling salesman problem* (TSP) serves as a quintessential instance, with numerous experts and academics having delved into its intricacies. After years of research on combinatorial optimization problems, intelligent algorithms, such as GAs [20, 21], ACOs [22–26], simulated annealing algorithms [27,28], artificial bee colony algorithms (ABC) [29,30], cuckoo search algorithms [31], and bat algorithms [32] have become the mainstream methods for solving this type of problem. Among the many intelligent search algorithms, the ACO is widely used because of its high search accuracy, simple structure, and good performance in solving combinatorial optimization problems. This work also improves the ACO and applies it to the path planning of free-form surface inspection.

To address the issues of slow search speeds and a propensity for local optima in the ACO, this research introduces several modifications. These include refining the initial pheromone distribution, adjusting the pheromone evaporation rate, and updating the pheromone update strategy, along with the integration of a local search tactic. The resulting *improved ant colony algorithm* (IACO) exhibits enhanced search directivity in the early phases of iteration, rapid convergence, a reduced likelihood of getting trapped in local optima, and improved search precision. Two intricate free-form surface workpieces were crafted, and a variety of MPs were randomly produced to evaluate the algorithm's efficacy. Comparative simulation and inspection experiments were conducted against the ACO, ABC, and GA.

The paper is arranged as follows. The Section 2 details the composition of the IP when the CMM inspects free-form surfaces and analyses the mathematical model of the IP to be optimized. Section 3 summarizes the basic structure of the ACO and introduces the specific strategies of the IACO in this paper. Section 4 discusses the experimental simulation results and experimental inspection results as well as analyses the experimental effects of the IACO. Section 5 provides a summary of the work of this paper. This paper is one of the outcomes of our research project. The scope of our research project is the efficient and high-precision inspection of free-form surfaces, with the aim of providing theoretical and technical support for precision inspection in the context of intelligent manufacturing.

2. Mathematical model of the free-form surface inspection path

When the CMM inspects free-form surfaces, the moving trajectory of the probe is as shown in Fig. 1. The figure only illustrates the probe movement process for two MPs, but other MPs can also be used as an example. At the beginning of the inspection work, the probe moves from the waiting position to the *positioning point* (PP) of the first MP (the PP aligns with the normal vector of the MP, at a certain safe distance from the MP), then approaches the MP along the normal direction of the MP, then retreats to the *retreat point* (RP), and moves to the next PP; the probe experiences changes in speed and acceleration during the movement and inspection process, reaching high positioning speed, touch inspection speed, and retreat speed.

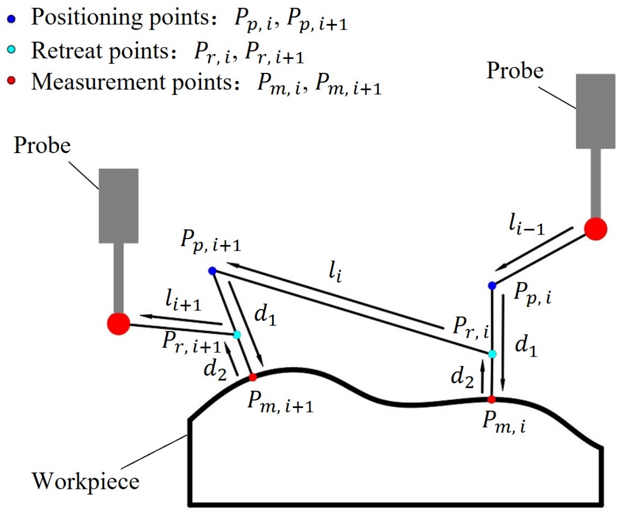
● Positioning points：$P_{p,\,i}$, $P_{p,\,i+1}$
○ Retreat points：$P_{r,\,i}$, $P_{r,\,i+1}$
● Measurement points：$P_{m,\,i}$, $P_{m,\,i+1}$
Probe
Probe
l_{i-1}
$P_{p,\,i+1}$
l_i
$P_{p,\,i}$
l_{i+1}
d_1
$P_{r,\,i}$
d_1
$P_{r,\,i+1}$
d_2
d_2
$P_{m,\,i+1}$
$P_{m,\,i}$
Workpiece

Fig. 1. Schematic diagram of the local inspection path on a free-form surface.

Figure 1 shows that when two MPs are inspected, the probe movement path can be divided into three subpaths, namely, d_1, d_2 and l_i. Among them, the distances d_1 and d_2 can be considered constant and are set by the experimental personnel for the equipment parameters, but l_i is not a constant value. Therefore, when inspection work is implemented, the total distance of the probe movement path is as follows:

$$D = (d_1 + d_2)\, n + \sum_{i=1}^{n-1} l_i \tag{1}$$

where n is the number of MPs, d_1 is the distance from the PP to the corresponding MP, d_2 is the distance from the corresponding RP to the MP, $l_i (i = 1, 2, \ldots, n-1)$ is the distance from the RP of MP i to the PP of MP $i + 1$, and D is the total distance of the probe movement trajectory when the equipment inspects n MPs.

When the CMM is performing inspection work, because the distance d_1 from the PP to the corresponding MP and the retreat distance d_2 are known fixed values, only the distance l_i between the RP of MP i and the PP of MP $i + 1$ needs to be optimized. To make the probe movement trajectory distance as short as possible during inspection work, it is necessary to optimize the total

MP distance L of n MPs, which can be taken as the optimization objective function and expressed as follows:

$$L = \sum_{i=1}^{n-1} l_i = \sum_{i=1}^{n-1} \sqrt{(x_{i+1} - x_i)^2 + (y_{i+1} - y_i)^2 + (z_{i+1} - z_i)^2}, \tag{2}$$

where (x_i, y_i, z_i) are the spatial coordinates of MP i and where $(x_{i+1}, y_{i+1}, z_{i+1})$ are the spatial three-dimensional coordinates of MP $i + 1$.

3. Overview and improvement of the ant colony algorithm

3.1. Classic ant colony algorithm

The ACO refers to the foraging behaviour of ants in nature, which discretizes the problem and optimizes it into a node model, abstracts the artificial ants to randomly traverse each node to construct possible solutions, and then uses a positive feedback mechanism to reasonably adjust the pheromone content of the search path to gradually search for the optimal solution. When the ACO is used to optimize the IP of free-form surfaces, it is assumed that m ants are randomly placed on n MPs; set C represents the node set of all MPs; d_{ij} represents the distance between MP i and MP j; and τ_{ij} represents the pheromone value on path (ij) at a certain moment, where $\eta_{ij} = 1/d_{ij}$ reflects the expected degree of ants transferring from MP i to MP j at a certain moment. The basic model of the ACO is as follows:

1. Pheromone initialization

$$\tau_{ij}(0) = \text{const}, \tag{3}$$

where $\tau_{ij}(0)$ means that at the initial moment, all paths have the same pheromone concentration; const is a constant.

2. State transition probability At moment t, ant k independently selects the next unvisited MP according to the transfer probability $P_{ij}^k(t)$ calculated by (4) and records the currently selected MP in the tabu$_k (k = 1, 2, \cdots, m)$ list:

$$P_{ij}^k(t) = \begin{cases} \text{allowed}_k = \{C - \text{tabu}_k\} & \\ \dfrac{[\tau_{ij}(t)]^\alpha \cdot [\eta_{tk}(t)]^\beta}{\sum\limits_{s \in \text{allowed}_k} [\tau_{is}(t)]^\alpha \cdot [\eta_{is}(t)]^\beta}, & j \in \text{allowed}_k \\ 0, & j \notin \text{allowed}_k \end{cases}, \tag{4}$$

where allowed$_k$ is the set of MPs that ant k can currently choose; α represents the pheromone heuristic factor, which indicates the extent to which pheromones affect the path chosen by the ants; β denotes the expected heuristic factor, signifying the significance of the heuristic function in determining the ants' path selection.

3. Pheromone update After all ants have completed a complete traversal, that is, they have independently completed the construction of a complete path solution, the pheromone on the nodes of the current feasible solution is updated according to (5):

$$\begin{cases} \tau_{ij}(t+1) = (1 - \rho) \cdot \tau_{ij}(t) + \Delta\tau_{ij}(t) \\ \Delta\tau_{ij}(t) = \sum\limits_{k=1}^{m} \Delta\tau_{ij}^k(t) \end{cases}, \tag{5}$$

where $\rho \in (0,1)$ is the pheromone evaporation coefficient; $\Delta\tau_{ij}(t)$ is the pheromone increment released by all ants on path (ij) during this search, which is usually defined by the ant cycle model via global path information updating:

$$\Delta\tau_{ij}^{k}t) = \begin{cases} \dfrac{Q}{L_k}, & k \in (i,j) \\ 0, & \text{others} \end{cases}, \tag{6}$$

where Q is the total amount of pheromone and where L_k is the path length searched by ant k in this search.

3.2. Improved ant colony algorithm

3.2.1. Improvement of the initial pheromone

In the ACO, when ants start searching, the initial pheromone of each search path is an equal constant value, which makes the ACO very blind at the beginning of the iteration, resulting in a low search speed. To enhance the algorithm's search capabilities during the early phases, the configuration of the initial pheromones has been optimized in the following manner:

$$\tau_{ij}(0) = \begin{cases} \dfrac{Q}{d_{ij}}, & \text{if} \quad i \neq j \\ 0, & \text{others} \end{cases}. \tag{7}$$

As depicted in (7), the initial pheromone concentration at each MP is set to be inversely related to the distance separating the MPs at the commencement of the iteration process, which gives the algorithm a certain directionality at the beginning of the iteration, effectively reducing the interference of invalid paths and increasing the search speed of the algorithm.

3.2.2. Improvement of the pheromone evaporation factor

The pheromone evaporation factor ρ is an important parameter that ascertains whether the ACO can search for the optimal solution because it determines the pheromone content on each search path after each iteration of the ACO. The value of the pheromone evaporation factor ρ should be set reasonably. If the pheromone evaporation rate is set too high, the pheromones on the paths identified during each cycle of the algorithm will dissipate rapidly. This can lead to the ACO converging too swiftly, which may result in the omission of potentially superior solutions. Conversely, if the evaporation rate is set too low, the ACO might become fixated on suboptimal solutions, thereby hindering the discovery of more optimal paths. Therefore, it is crucial to adjust the pheromone evaporation rate to an optimal level that prevents premature convergence while avoiding stagnation in local optima. This section improves the pheromone evaporation factor ρ so that it conforms to the normal distribution. The advantage of the improvement is that at the beginning of the iteration, the pheromone is an important reference for ants to choose the search path, so a smaller pheromone evaporation factor ρ value can ensure that the algorithm passes through the initial iteration quickly and increases the search speed. During the central phase of the algorithm's iterative process, the pheromone levels on each potential path remain relatively stable, with minimal numerical fluctuations. This constancy can lead the ACO to a local optimum. At this juncture, increasing the pheromone evaporation factor ρ can enlarge the solution space explored by the ants, facilitating an escape from local optima. As the iteration process advances, once all probable paths that could contain the optimal solution have been explored, the optimal solution is ascertained. At this point, reducing the pheromone evaporation factor ρ enhances the pheromones' guiding influence, thereby hastening the algorithm's convergence towards the optimal solution. The improved pheromone evaporation factor is determined by (8):

$$\rho(k) = \frac{1}{\sqrt{2\pi}\sigma} e^{-\frac{(k_\mathrm{b}-\mu)^2}{2\sigma^2}}, \tag{8}$$

where k_b is the index of the ant that has currently found the shortest path.

$$\mu = \frac{\sum\limits_{k=1}^{m} \tau_{k_\mathrm{b}}}{m}, \tag{9}$$

$$\sigma = \frac{\sum\limits_{k=1}^{m} \left(\tau_{ij} - \mu\right)^2}{m}. \tag{10}$$

where τ_{k_b} is the pheromone amount of the shortest path currently found by the ant; μ is the average pheromone amount of the shortest path found by the ant after completing one iteration; σ is the variance of the pheromone amounts of the best path and the worst path after completing one iteration; and m is the total number of ants.

3.2.3. Differentiated pheromone updating strategy

The positive feedback mechanism significantly influences the iterative search routine of the ACO, dictating the search trajectory of each ant during every iteration by modulating the pheromones along the potential paths. The downside is that the adjustment of pheromones only takes the path length as a reference standard and does not evaluate the quality of all known paths, which makes the adjustment blind and leads to a decrease in the search speed of the algorithm. Therefore, this section improves the pheromone updating strategy. After each iteration is completed, the best path length L_best, the worst path length L_worst, and the average path length L_ave are calculated; then, a certain amount of pheromone incentive is given to the better paths with lengths less than L_ave, and the pheromone amount of the worse paths with lengths greater than L_ave is reduced. The pheromone increment is calculated via (11):

$$\Delta\tau_{ij}^{k}(t) = \begin{cases} \dfrac{L_\mathrm{ave} - L_k}{L_\mathrm{ave} - L_\mathrm{best}} \cdot \dfrac{1}{L_k}, & L_k \le L_\mathrm{ave} \\ -\dfrac{L_k - L_\mathrm{ave}}{L_\mathrm{ave} - L_\mathrm{best}} \cdot \dfrac{1}{L_\mathrm{worst}}, & L_k > L_\mathrm{ave}, \end{cases} \tag{11}$$

where $\Delta\tau_{ij}^{k}(t)$ is the path length of ant k found in this iteration and L_k is the average path length after this iteration is completed.

To ensure that the ants in the next iteration continue to search along the better paths, the shortest path found in each iteration is given a pheromone reward $\Delta\tau_{ij}^{*}$, and the improved pheromone updating strategy is shown in (12), where it is calculated according to (13):

$$\tau_{ij}(t+1) = (1-\rho) \cdot \tau_{ij}(t) + \Delta\tau_{ij}(t) + \Delta\tau_{ij}^{*}, \tag{12}$$

$$\Delta\tau_{ij}^{*} = \frac{Q}{L_\mathrm{best}}. \tag{13}$$

Equations (11) to (13) adjust the pheromones on the basis of the known quality of each path. Positive feedback adjustment is applied to better IPs, and negative feedback adjustment is applied to worse IPs, resulting in a differentiated adjustment of IP pheromones which exploits the better paths that have been searched and increases the search speed of the algorithm to a certain extent.

3.2.4. Local search strategy

To boost the ACO's capability to escape local optima and to refine its search precision, a local exploration is conducted on superior paths that exhibit path lengths below the average value L_{ave} during each cycle of iteration. First, two random numbers r_1 and $r_2 (r_1 \neq r_2, r_1 \geq 1, r_2 \leq n)$ are generated via logistic chaotic mapping, and MPs r_1 and r_2 on the path are swapped. If the new path length is shorter after the position exchange, the result is accepted; otherwise, it is not. The principle of the local search strategy is represented by (14) to (15):

$$R = \{P(1), P(2), \cdots, P(r_1), P(r_1 + 1), \cdots, P(r_2), P(r_2 + 1), \cdots, P(n)\}, \tag{14}$$

$$R' = \{P(1), P(2), \cdots, P(r_2), P(r_1 + 1), \cdots, P(r_1), P(r_2 + 1), \cdots, P(n)\}, \tag{15}$$

where R is an IP with a path length less than L_{ave}; R' is the new IP after the local search; $P(n)$ represents MP n on a certain path; and $n(n \geq 2)$ is the number of MPs.

3.2.5. Steps of the improved ant colony algorithm

Upon incorporating the aforementioned enhancements into the ACO, the improved version, referred to as IACO, demonstrates superior search capabilities and increased search velocity compared with the original ACO. The detailed procedure of the IACO is outlined below, with a corresponding flowchart depicted in Fig. 2.

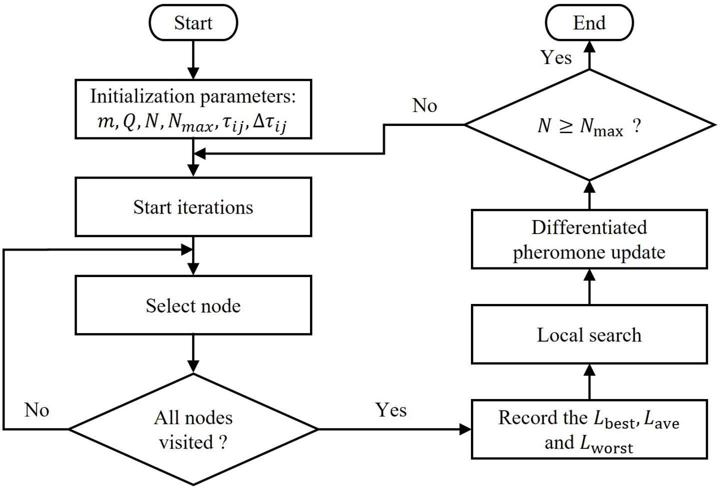
Start
Initialization parameters: $m, Q, N, N_{max}, \tau_{ij}, \Delta\tau_{ij}$
Start iterations
Select node
All nodes visited ?
No
Yes
Record the $L_{\text{best}}, L_{\text{ave}}$ and L_{worst}
Local search
Differentiated pheromone update
$N \geq N_{\max}$?
No
Yes
End

Fig. 2. Flowchart of the improved ant colony algorithm.

Step 1: The parameters are initialized. The number of ants m and pheromone total Q are initialized, the maximum number of iterations $N_{\max}$ is set, the initial pheromone concentration $\tau_{ij}(0)$ of each path is calculated according to (7), the initial pheromone increment $\Delta\tau_{ij}(0) = 0$ is set, and the tabu list is initialized such that it is empty.

Step 2: The initial positions of m ants from n MPs are randomly selected and added to the tabu list.

DOI: 10.24425/mms.2025.154343

Step 3: Each ant selects the next MP according to (4) and updates the tabu list.

Step 4: If each MP has been traversed, the shortest path L_{best}, the longest path L_{worst}, and the average path L_{ave} are recorded.

Step 5: According to (14) and (15), a local search is performed on the better paths with lengths less than L_{ave}. If the new path is shorter, it is accepted, and the path record is updated; otherwise, it is not.

Step 6: The pheromone concentration of each path is updated according to (11) to (13).

Step 7: It is ascertained whether the iteration has attained the maximum allowable count. If it has, the iteration is ended, and the shortest path is output; otherwise, Step 2 is repeated, and the next iteration is started.

4. Experiments and analysis of results

4.1. Simulation experiment

To assess the practicality of the IACO within this study, two specimens with intricate free-form surfaces were fabricated for simulation purposes, as illustrated in Fig. 3. Here, the base dimensions of Workpiece 1 are 110 mm × 110 mm × 8.2 mm and the main body dimensions are 80 mm × 80 mm × 7.3 mm; while the base dimensions and main body dimensions of Workpiece 2 are 120 mm × 120 mm × 10 mm and 100 mm × 100 mm × 75.9 mm, respectively. The figure shows that there is a large difference in the complexity of the two workpieces, among which workpiece (b) has a more complex surface shape, a large span in the height direction, and a large change in curvature. To simulate complex inspection conditions, MPs were randomly generated on each surface model, taking 200 MPs as an example, as shown in Fig. 4.

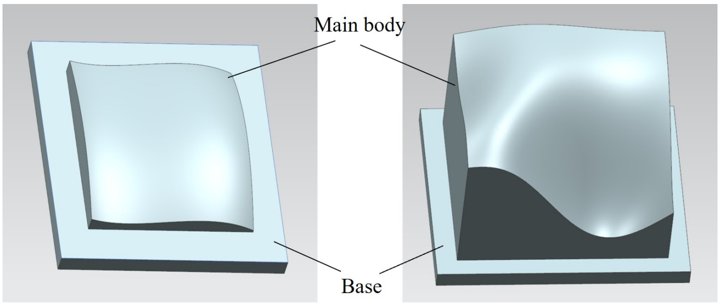

Fig. 3. CAD model for the simulation experiment: Workpiece 1 (left) and Workpiece 2 (right).

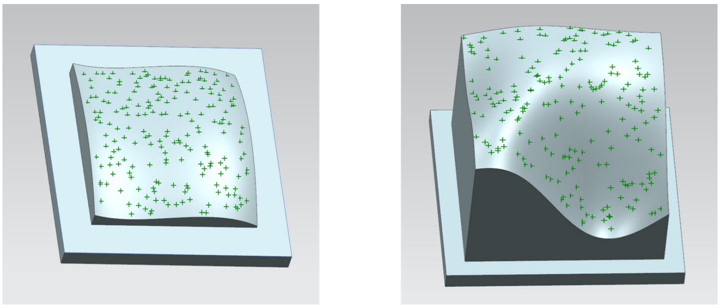

Fig. 4. MP distribution: Workpiece 1 (left) and Workpiece 2 (right).

The program was written in MATLAB 2022b software, and the IACO was compared with the ACO, GA, and ABC. The algorithm parameters were set as follows: $m = 30$, $Q = 30$, $N = 0$, $N_{\max} = 500$ and $\tau_{ij}(0) = 0$. For illustrative purposes, this study utilizes 200 MPs that are randomly dispersed to exemplify the optimization process. Figures 5 and 6 present the optimization outcomes for the IP of two free-form surface workpieces, labelled as Workpiece 1 and Workpiece 2, respectively, using a variety of optimization algorithms. Additionally, Fig. 7 illustrates the iterative progression of each optimization algorithm as they perform IP optimization on the two workpieces.

Figures 5 and 6 show that, compared with those of the ACO, GA, and ABC, the IP optimized by the IACO is neater and more aesthetically pleasing, and there is no local intersection in the IP, which can effectively reduce unnecessary IP consumption. The iterative process of the various algorithms in Fig. 7 shows that, compared with the ACO, the IACO has a better initial solution due to the reasonable improvement in the initial pheromone distribution, has a strong search directionality, and can search for the optimal solution more quickly. Thanks to the application of a differentiated pheromone update approach and an optimal pheromone evaporation rate, the IACO manages to secure a higher quality of optimal solutions. In contrast, the ACO frequently encounters issues with local optima and suffers from reduced search precision. The GA exhibits a sluggish convergence rate and inferior solution quality, with a propensity for a decline in population diversity as the iteration progresses. Meanwhile, the ABC exhibits a heightened dependency on the initial solution, and while it demonstrates better convergence and search accuracy than the GA, it still falls short when compared to the IACO. In conclusion, the IACO demonstrates superior overall performance over the ACO, GA, and ABC, showcasing robust directional search capabilities early in the iteration process, rapid convergence, robustness against local optima, and high search precision.

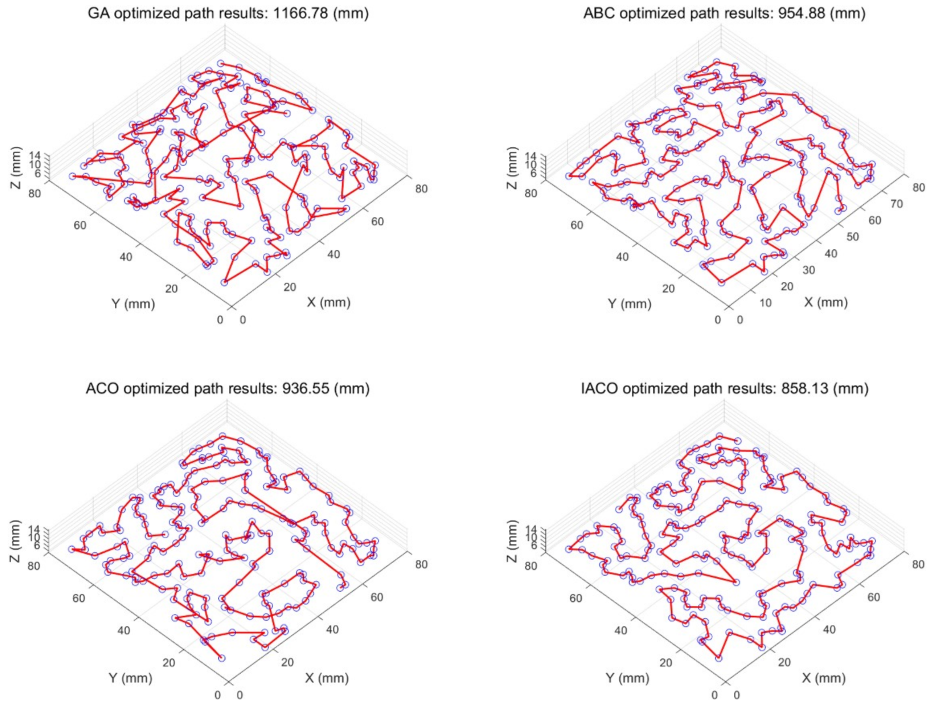

Fig. 5. Optimization results of the inspection path for Workpiece 1 via various algorithms.

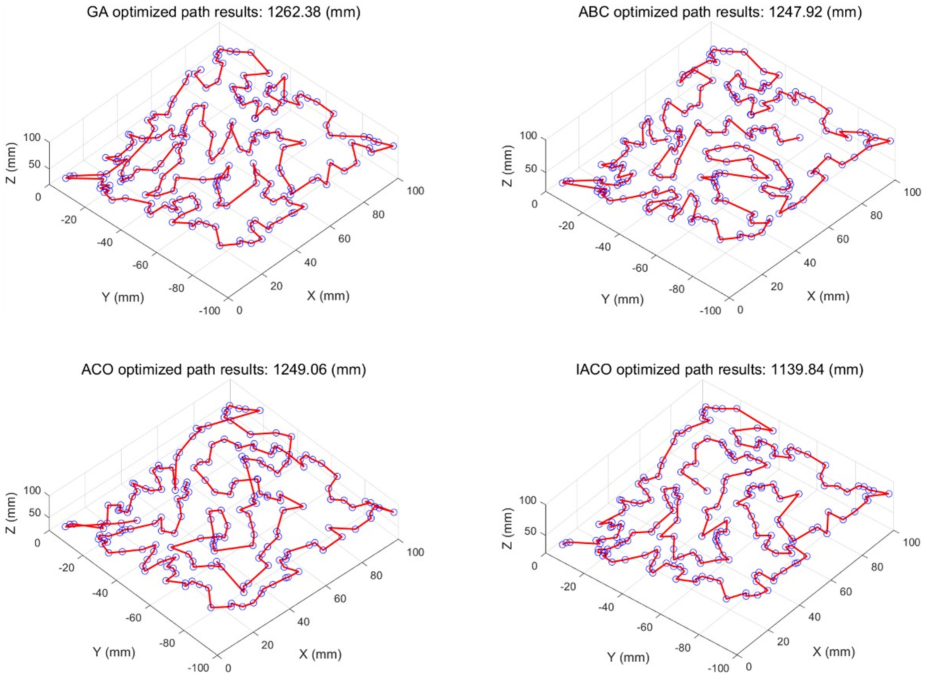

Fig. 6. Optimization results of the inspection path for Workpiece 2 via various algorithms.

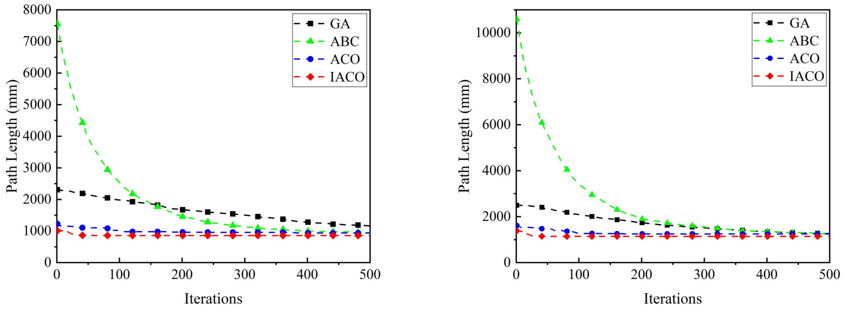

Fig. 7. Iteration process of various algorithms for optimizing the inspection path: Workpiece 1 (left) and Workpiece 2 (right).

Table 1 shows the experimental simulation results of different MP quantities for the two free-form surface workpieces. In the text, D_{IACO} represents the IP length optimized by the IACO, with the optimization results of the other algorithms following suit. Compared with that optimized by the ACO, when the MPs is 100, the IP optimized by the IACO is shortened by at least 2.2% and by 2.41% at most; when the MPs is 200, the IP optimized by the IACO is shortened by at least 8.37% and 8.74% at most; and when the MPs is 300, the IP optimized by the IACO is shortened by at least 3.53% and 9.29% at most. Compared with that optimized by the ABC, when the MPs are 100, 200, and 300, the IP optimized by the IACO is shortened by 3.85%, 10.13%, and 28.68% at most, respectively; compared with that optimized by the GA, when the MPs are 100, 200, and 300, the IP optimized by the IACO is shortened by 9.18%, 26.45%, and 48.9% at most, respectively.

Table 1. Simulation results for different MP quantities on each workpiece.

Results	**Workpiece 1**			**Workpiece 2**		
MPs	100	200	300	100	200	300
D_{GA}(mm)	681.85	1166.78	2261.33	907.62	1262.38	2198.03
D_{ABC}(mm)	627.47	954.88	1570.25	863.87	1247.92	1574.01
D_{ACO}(mm)	634.54	936.55	1203.26	849.23	1249.06	1237.53
D_{IACO}(mm)	619.25	858.13	1160.75	830.58	1139.84	1122.52
$1 - D_{\mathrm{IACO}}/D_{\mathrm{GA}}$	9.18%	26.45%	48.67%	8.49%	9.71%	48.9%
$1 - D_{\mathrm{IACO}}/D_{\mathrm{ABC}}$	1.31%	10.13%	26.08%	3.85%	8.66%	28.68%
$1 - D_{\mathrm{IACO}}/D_{\mathrm{ACO}}$	2.41%	8.37%	3.53%	2.2%	8.74%	9.29%

Table 2 shows the time spent on optimizing the IP by each optimization algorithm. In the text, $T_{\mathrm{R-IACO}}$ represents the time expenditure of the IACO, with the time costs of the other algorithms being analogous. The data in Table 2 indicate that because the IACO has a good search directionality from the beginning of the iteration, the time required for optimization is relatively short.

Table 2. Time spent on optimizing the inspection path by different optimization algorithms.

Results	**Workpiece 1**			**Workpiece 2**		
MPs	100	200	300	100	200	300
$T_{\mathrm{R-GA}}$ (s)	69	135	187	72	133	191
$T_{\mathrm{R-ABC}}$ (s)	95	198	310	97	196	305
$T_{\mathrm{R-ACO}}$ (s)	59	113	165	61	111	162
$T_{\mathrm{R-IACO}}$ (s)	37	41	54	38	43	58

4.2. Inspection experiment

Free-form surface Workpiece 1 and Workpiece 2 were placed on a *German Hexagon Leitz Reference HP CMM* for inspection experiments. The software used by this CMM is PC-DMIS. The accuracy of the CMM: $\mathrm{MPE_E} = 0.9 + L/400\mu m$. The diameter of the probe standard is 5 mm, and the positioning distance and retreat distance of the probe are both 10 mm. The moving speed of the probe is set to 20 mm/s. The IPs optimized by the IACO, ACO, GA, and ABC were experimentally inspected. The experimental process is shown in Fig. 8, and the IT spent on each workpiece is shown in Table 3. Table 4 shows the total time spent on each optimization algorithm, where $T_{\mathrm{T-IACO}}$ represents the total time spent by the IACO, including the time spent on the optimization process $T_{\mathrm{R-IACO}}$ and the inspection process $T_{\mathrm{I-IACO}}$, and the time spent by the other optimization algorithms is similarly defined.

Table 3 shows that under basically the same experimental conditions, the shorter the IP of the free-form surface, the shorter the IT required for the CMM inspection experiment. Among them, the IP optimized by the IACO takes the shortest IT. Compared with that optimized by the ACO, when the MPs is 100, the IT of the IP optimized by the IACO is shortened by at least 5.08% and 5.27% at most; when the MPs is 200, the IT of the IP optimized by the IACO is shortened by at least 10.85% and 10.86% at most; and when the MPs is 300, the IT of the IP optimized by the IACO is shortened by at least 14.42% 14.75% and at most. Compared with that improved by the ABC, when the MPs are 100,

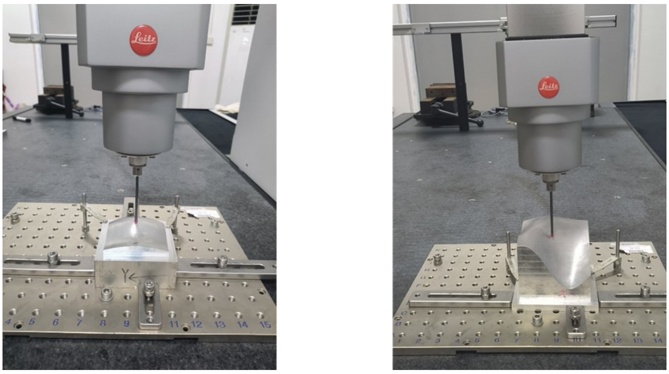

Fig. 8. CMM inspection process: Workpiece 1 (left) and Workpiece 2 (right).

Table 3. Inspection time for different inspection paths.

Results	**Workpiece 1**			**Workpiece 2**		
MPs	100	200	300	100	200	300
$T_{\mathrm{I-GA}}$ (s)	620	1176	2540	709	1149	2668
$T_{\mathrm{I-ABC}}$ (s)	580	1090	2038	678	1132	2215
$T_{\mathrm{I-ACO}}$ (s)	586	1075	1771	667	1133	1873
$T_{\mathrm{I-IACO}}$ (s)	574	1018	1605	653	1066	1598

Table 4. Total time spent and efficiency comparison.

Results	**Workpiece 1**			**Workpiece 2**		
MPs	100	200	300	100	200	300
$T_{\mathrm{T-GA}}$ (s)	689	1311	2727	781	1282	2859
$T_{\mathrm{T-ABC}}$ (s)	675	1288	2348	775	1328	2520
$T_{\mathrm{T-ACO}}$ (s)	645	1188	1946	728	1244	1935
$T_{\mathrm{T-IACO}}$ (s)	611	1059	1659	691	1109	1656
$1 - T_{\mathrm{T-IACO}}/T_{\mathrm{T-GA}}$	11.32%	19.22%	34.21%	11.52%	13.49%	32%
$1 - T_{\mathrm{T-IACO}}/T_{\mathrm{T-ABC}}$	9.48%	17.78%	23.59%	10.84%	16.49%	22.86%
$1 - T_{\mathrm{T-IACO}}/T_{\mathrm{T-ACO}}$	5.27%	10.86%	14.75%	5.08%	10.85%	14.42%

200, and 300, the IT of the IP optimized by the IACO is shortened by 10.84%, 17.78%, and 23.59% at most, respectively; compared with that optimized. By the GA, when the MPs are 100, 200, and 300, the IT of the IP optimized by the IACO is shortened by 11.52%, 19.22%, and 34.21% at most, respectively. On the other hand, the data in Table 1 show that the more MPs there are in the optimization of the IP of the free-form surface workpiece by the IACO, the more obvious the optimization effect.

5. Conclusions

To address the disordered IPs and long IT encountered when CMMs inspect free-form surface parts, this work uses the IACO for the IP planning of free-form surfaces, which can effectively shorten the IP and time. The ACO suffers from prolonged search duration and susceptibility to getting trapped in local optima. This work has made improvements, including ones in the initial pheromone distribution, the pheromone evaporation factor, the pheromone update strategy, as well as introduced a local search strategy. After simulation experiments and inspection experiments, compared with those optimized by the ACO, ABC and GA, the inspection efficiency optimized by the IACO increased by up to 14.75%, 23.59% and 34.21%, respectively. The experimental results show that the IACO of this paper can improve the work efficiency when the CMM inspects free-form surfaces and can effectively shorten the IT.

However, the factors that determine the inspection efficiency of free-form surfaces are not only the length of the IP but there are also others closely related to the number and distribution of MPs. In the actual inspection of free-form surfaces, only a reasonable number of MPs and an appropriate layout can accurately reflect the form error of free-form surfaces. The experiments in this paper used 100, 200, and 300 randomly distributed MPs, which cannot fully reflect the errors of free-form surfaces. This paper merely provides a reference algorithm for optimizing the IP of free-form products (such as blades, impellers, moulds, etc.) to further improve inspection efficiency. The actual number and layout of MPs used in the inspection process should still be determined based on specific circumstances. This paper does not consider the impact of different numbers and layouts of MPs on the inspection accuracy of free-form surfaces, and the IACO proposed in this paper is only applicable to the optimization of IPs for free-form surfaces with a small number of MPs. Therefore, for future work, we will explore large-scale MP inspection technologies for free-form surfaces and include the impact of different numbers and distributions of MPs on the inspection accuracy of free-form surfaces in the scope of consideration.

Acknowledgements

This work was financially supported by the National Nature Science Foundation of China (51565006, 52165054), the Natural Science Foundation of the Guangxi Province (2025GXNSFHA069171), the Science Research Innovation Team Project of the Guangxi Provincial Education Department, and the Science Research Innovation Team Project of Guangxi University of Science and Technology.

References

[1] Zahmati, J., Amirabadi, H., & Mehrad, V. (2018). A hybrid measurement sampling method for accurate inspection of geometric errors on freeform surfaces. *Measurement*, *122*, 155–167. https://doi.org/10.1016/j.measurement.2018.03.013

[2] Kamrani, A., Nasr, E.A., Al-Ahmari, A., Abdulhameed, O., & Mian, S.H. (2014). Feature-based design approach for integrated CAD and computer-aided inspection planning. *The International Journal of Advanced Manufacturing Technology*, *76*(9–12), 2159–2183. https://doi.org/10.1007/s00170-014-6396-0

[3] Abdulhameed, O., Mian, S.H., Al-Ahmari, A., & Alkhalefah, H. (2020). Patch and curvature specific estimation of efficient sampling scheme for complex surface inspection. *The International Journal of Advanced Manufacturing Technology*, *110*(11–12), 3407–3422. https://doi.org/10.1007/s00170-020-06063-6

[4] He, G., Sang, Y., Pang, K., & Sun, G. (2018). An improved adaptive sampling strategy for freeform surface inspection on CMM. *The International Journal of Advanced Manufacturing Technology*, *96*(1–4), 1521–1535. https://doi.org/10.1007/s00170-018-1612-y

[5] Teodor, V.G., Păunoiu, V., Susac, F., & Baroiu, N. (2019). Optimization of the measurement path for the car body parts inspection. *Measurement*, *146*, 15–23. https://doi.org/10.1016/j.measurement.2019.06.002

[6] Li, B., Feng, P., Zeng, L., Xu, C., & Zhang, J. (2018). Path planning method for on-machine inspection of aerospace structures based on adjacent feature graph. *Robotics and Computer-Integrated Manufacturing*, *54*, 17–34. https://doi.org/10.1016/j.rcim.2018.05.006

[7] Liu, Y., Zhao, W., Sun, R., & Yue, X. (2020). Optimal path planning for automated dimensional inspection of free-form surfaces. *Journal of Manufacturing Systems*, *56*, 84–92. https://doi.org/10.1016/j.jmsy.2020.05.008

[8] Tsagaris, A., & Mansour, G. (2019). Path planning optimization for mechatronic systems with the use of genetic algorithm and ant colony. *IOP Conference Series Materials Science and Engineering*, *564*(1), 012051. https://doi.org/10.1088/1757-899x/564/1/012051

[9] Yi, B., Qiao, F., Hua, L., Wang, X., Wu, S., & Huang, N. (2022). Touch Trigger Probe-Based Interference-Free Inspection Path Planning for Free-form Surfaces by Optimizing the Probe Posture. *IEEE Transactions on Instrumentation and Measurement*, *71*, 1–8. https://doi.org/10.1109/tim.2022.3147314

[10] Li, Y., Zeng, L., Tang, K., & Xie, C. (2019). Orientation-point relation based inspection path planning method for 5-axis OMI system. *Robotics and Computer-Integrated Manufacturing*, *61*, 101827. https://doi.org/10.1016/j.rcim.2019.101827

[11] Abdulhameed, O., Al-Ahmari, A., Mian, S.H., & Aboudaif, M.K. (2020). Path planning and setup orientation for automated dimensional inspection using coordinate measuring machines. *Mathematical Problems in Engineering*, *2020*, 1–17. https://doi.org/10.1155/2020/9683074

[12] Han, Z., Liu, S., Yu, F., Zhang, X., & Zhang, G. (2017). A 3D measuring path planning strategy for intelligent CMMs based on an improved ant colony algorithm. *The International Journal of Advanced Manufacturing Technology*, *93*(1–4), 1487–1497. https://doi.org/10.1007/s00170-017-0503-y

[13] Stojadinovic, S.M., Majstorovic, V.D., Durakbasa, N.M., & Sibalija, T.V. (2016). Ants colony optimisation of a measuring path of prismatic parts on a CMM. *Metrology and Measurement Systems*, *23*(1), 119–132. https://doi.org/10.1515/mms-2016-0011

[14] Zhao, Z., Li, Y., & Fu, Y. (2022). Collision-free path planning for efficient inspection of free-form surface by using a trigger probe. *The International Journal of Advanced Manufacturing Technology*, *120*(3–4), 2183–2200. https://doi.org/10.1007/s00170-022-08917-7

[15] Zakharov, O., Balaev, A., & Kochetkov, A. (2017). Modeling Optimal Path of Touch Sensor of Coordinate Measuring Machine Based on Traveling Salesman Problem Solution. *Procedia Engineering*, *206*, 1458–1463. https://doi.org/10.1016/j.proeng.2017.10.661

[16] He, G., Huang, X., Ma, W., Sang, Y., & Yu, G. (2016). CAD-based measurement planning strategy of complex surface for five axes on machine verification. *The International Journal of Advanced Manufacturing Technology*, *91*(5–8), 2101–2111. https://doi.org/10.1007/s00170-016-9932-2

[17] Zhao, W., Wang, X., & Liu, Y. (2022). Path planning for 5-Axis CMM inspection considering path reuse. *Machines*, *10*(11), 973. https://doi.org/10.3390/machines10110973

[18] Han, Z., Liu, S., Li, X., Wang, Y., Zhang, X., & Zhang, G. (2018). Path planning method for intelligent CMMs based on safety and the high-efficiency principle. *The International Journal of Advanced Manufacturing Technology*, *95*(9–12), 4003–4012. https://doi.org/10.1007/s00170-017-1500-x

[19] Lin, C., & Lin, C. (2019). An adaptive-group-based differential evolution algorithm for inspecting machined workpiece path planning. *The International Journal of Advanced Manufacturing Technology*, *105*(5–6), 2647–2657. https://doi.org/10.1007/s00170-019-04521-4

[20] Zhang, P., Wang, J., Tian, Z., Sun, S., Li, J., & Yang, J. (2022). A genetic algorithm with jumping gene and heuristic operators for traveling salesman problem. *Applied Soft Computing*, *127*, 109339. https://doi.org/10.1016/j.asoc.2022.109339

[21] Jain, R., Singh, K.P., Meena, A., Rana, K.B., Meena, M.L., Dangayach, G.S., & Gao, X. (2022). Application of proposed hybrid active genetic algorithm for optimization of traveling salesman problem. *Soft Computing*, *27*(8), 4975–4985. https://doi.org/10.1007/s00500-022-07581-z

[22] Yang, K., You, X., Liu, S., & Pan, H. (2020). A novel ant colony optimization based on game for traveling salesman problem. *Applied Intelligence*, *50*(12), 4529–4542. https://doi.org/10.1007/s10489-020-01799-w

[23] Xiao, Z., Wang, Z., Liu, D., & Wang, H. (2021). A path planning algorithm for PCB surface quality automatic inspection. *Journal of Intelligent Manufacturing*, *33*(6), 1829–1841. https://doi.org/10.1007/s10845-021-01766-3

[24] Liu, H., Lee, A., Lee, W., & Guo, P. (2023). DAACO: adaptive dynamic quantity of ant ACO algorithm to solve the traveling salesman problem. *Complex & Intelligent Systems*, *9*(4), 4317–4330. https://doi.org/10.1007/s40747-022-00949-6

[25] Chen, J., Zheng, K., Li, Q., & Ayush, A. (2022). Influence of subproblem solutions on the quality of traveling thief problem solutions. *Journal of Intelligent & Fuzzy Systems*, *44*(2), 1943–1956. https://doi.org/10.3233/jifs-221032

[26] Gao, W. (2020). Modified ant colony optimization with improved tour construction and pheromone updating strategies for traveling salesman problem. *Soft Computing*, *25*(4), 3263–3289. https://doi.org/10.1007/s00500-020-05376-8

[27] İlhan, İ., & Gökmen, G. (2022). A list-based simulated annealing algorithm with crossover operator for the traveling salesman problem. *Neural Computing and Applications*, *34*(10), 7627–7652. https://doi.org/10.1007/s00521-021-06883-x

[28] Wang, L., Cai, R., Lin, M., & Zhong, Y. (2019). Enhanced List-Based Simulated Annealing Algorithm for Large-Scale Traveling Salesman Problem. *IEEE Access*, *7*, 144366–144380. https://doi.org/10.1109/access.2019.2945570

[29] Khan, I., & Maiti, M.K. (2018). A swap sequence based Artificial Bee Colony algorithm for Traveling Salesman Problem. *Swarm and Evolutionary Computation*, *44*, 428–438. https://doi.org/10.1016/j.swevo.2018.05.006

[30] Choong, S.S., Wong, L., & Lim, C.P. (2018). An artificial bee colony algorithm with a Modified Choice Function for the traveling salesman problem. *Swarm and Evolutionary Computation*, *44*, 622–635. https://doi.org/10.1016/j.swevo.2018.08.004

[31] Ouaarab, A., Ahiod, B., & Yang, X. (2013). Discrete cuckoo search algorithm for the travelling salesman problem. *Neural Computing and Applications*, *24*(7–8), 1659–1669. https://doi.org/10.1007/s00521-013-1402-2

[32] Osaba, E., Yang, X., Diaz, F., Lopez-Garcia, P., & Carballedo, R. (2015). An improved discrete bat algorithm for symmetric and asymmetric Traveling Salesman Problems. *Engineering Applications of Artificial Intelligence*, *48*, 59–71. https://doi.org/10.1016/j.engappai.2015.10.006

DOI: 10.24425/mms.2025.154343

Yueping Chen received the Ph.D. degree in mechanical engineering from Guangdong University of Technology, Guangzhou, China, in 2012. He is currently a Professor with Guangxi University of Science and Technology Liuzhou, Guangxi, China. His research interests include precision engineering and machining error compensation.

Sian Wei is currently studying for his M.Sc. degree in engineering at Guangxi University of Science and Technology Liuzhou, Guangxi, China. His research interests are precision inspection technology and freeform surfaces inspection path planning.

Jiegao Ma received the B.Sc. degree in automotive engineering from Tongji University, China. From 2007 to 2024, he held engineering positions in the Dongfeng Liuzhou Motor Co., Ltd. where he was involved in developing engines and power train systems for vehicles.